Eur. J. Mineral.
2007, **19**, 499–511
Published online August 2007

Amphibole crystallization in the Etnean feeding system: mineral chemistry and trace element partitioning between Mg-hastingsite and alkali basaltic melt

MARCO VICCARO, CARMELO FERLITO and RENATO CRISTOFOLINI*

Dipartimento di Scienze Geologiche, Università di Catania, Corso Italia 57, 95129 Catania, Italy
*Corresponding author, e-mail: rcristof@unict.it

Abstract: Amphiboles are rather rare in the volcanics of the whole Etnean succession and commonly are represented by kaersutites to titanian pargasites, mostly found in differentiated products. Titanian Mg-hastingsites have been found in lavas and tephra from the 2001 eruption at Mt. Etna. New major (EMPA) and trace element (LAM-ICP/MS) data on amphiboles from this eruption have been compared with reference data for kaersutites from prehistoric eruptions. The two amphibole groups significantly differ from each other in their Al^{IV}, Al^{VI}, K and Mg# values, which are higher in Mg-hastingsite than in kaersutite. Ti and Na are lower in Mg-hastingsite than in kaersutite. REE and trace element patterns for all the analysed Mg-hastingsite crystals are quite homogeneous. Kaersutite patterns generally conform to those of Mg-hastingsite but display higher concentrations for most of the trace elements.

The exceptional occurrence, exclusively in tephra, of some crystals under equilibrium conditions with the coexisting residual glass has made it possible to calculate the partition coefficients between amphibole and melt ($^{Amph/melt}D$) for trace elements. A new set of partition coefficients is then provided, deriving from analyses on five amphibole/melt pairs at equilibrium. These data highlight the effects of amphibole crystallization in controlling some trace element ratios (*e.g.* Th (or U)/Ta, Th/Nb, La/Nb) in residual melts of alkali basaltic systems, and suggest new hints for interpreting possible geochemical anomalies of these magmas.

In addition, the comparison between the calculated $^{Amph/melt}D$ of Mg-hastingsite and those from literature relative to kaersutite from prehistoric eruptions shows that they are generally lower in the former than in the latter one for most of the trace elements. All of the available data provide constraints on the physical growth conditions for the 2001 Mg-hastingsite. Temperatures around 980 °C and volatile pressures in the range of 200−300 MPa have been estimated by integrating geophysical and petrological data. The highest pressure values are however larger than the lithostatic pressure alone acting on the magma reservoir (~ 6 km b.s.l.), as defined on the grounds of the hypocentres depth of the seismic events associated to the magma rise. This implies that Mg-hastingsite was probably crystallizing in a closed reservoir under overpressure conditions. Finally, micro-chemical data and trace element partitioning suggest that the differences between Mg-hastingsites and kaersutites in the Etnean products are mainly due to the less differentiated character of the magmas emitted after the 1971, and particularly after the 2001 eruption, compared to the compositions that characterize products of the prehistoric events. Furthermore, also a higher pressure of the system where Mg-hastingsite crystallized would account for its compositional differences respect to prehistoric kaersutite.

Key-words: Mt. Etna, partition coefficients, Mg-hastingsite, kaersutite, alkali basalts.

1. Introduction

Integrated minerochemical investigations on intratelluric phases of volcanic products have recently proved to be a powerful tool to constrain chemical and physical conditions controlling their crystallization, and to give therefore information on the timing of magma ascent before and during the eruption (Sato *et al.*, 1999; Nakagawa *et al.*, 2002; Reubi *et al.*, 2002; Couch *et al.*, 2003; Devine *et al.*, 2003; Rutherford & Devine, 2003; Barclay & Carmichael, 2004; Browne *et al.*, 2006). Furthermore, a proper choice of distribution coefficients for trace elements between mineral phases and silicatic melts is considered fundamental in order to develop accurate modelling of melting or crystal fractionation processes. Since hydrous phases (such as amphibole) generally have high distribution coefficients, their geochemical signature on the erupted magma will be clear, when they crystallize. However, the definition of $^{Amph/melt}D$ in natural magmatic systems sets some problems mainly related to the amphibole stability at low pressures. Amphibole is not stable at 0.1 MPa, therefore phenocrysts tend to re-equilibrate with the residual melt if the magma ascends at low rates. On the other hand, if magma is supplied by pulses that quickly reach the surface, hydrous phases such as amphibole might retain conditions close to the original thermodynamic equilibrium with the hosting melt. When the melt is quenched into glass, micro-analytical data on it and the mineral allow then reliable distribution coefficients to be calculated.

This occurred when an amphibole-bearing trachybasalt was erupted during the 2001 event on the southern flank of Mount Etna (Italy). Petrographic evidence has shown

DOI: 10.1127/0935-1221/2007/0019-1747
0935-1221/07/0019-1747 $ 5.85

that amphibole crystals in tephra produced by the most explosive phases of activity at one of the vents (Laghetto, 2550 m a.s.l.) do not have reaction rims, due to the fast magma ascent. The quenched glassy groundmass does represent the actual melt in equilibrium with the growing crystals at depth and $^{Amph/melt}D$ values can be then precisely defined. Models of differentiation processes of Etnean magmas, with broader implications for other alkali basaltic systems, may consequently be based also on $^{Amph/melt}D$, related to actual mineral and melt compositions, rather than on theoretical ones at times defined for quite distinct systems.

Amphibole found in the Etnean products, defined as *kaersutite* on the basis of its optical characters (Aoki, 1963), commonly displays a kaersutitic to titanian pargasitic chemistry (Klerkx, 1964; 1968; Cristofolini & Lo Giudice, 1969; Tanguy, 1980; Cristofolini *et al.*, 1981; D'Orazio *et al.*, 1998). It is rather rare in older prehistoric and historic volcanic rocks, and was last found in the products of the 1892 eruption (Clocchiatti & Tanguy, 2001). Among the products of the 2001 event, amphibole was found in either lavas or tephra and may mostly be defined as *titanian Mg-hastingsite* (Leake *et al.*, 1997), being quite distinct in its composition compared to phenocrysts of previous eruptions. Therefore, microchemical data and $^{Amph/melt}D$ on this Mg-hastingsite were compared with values related to kaersutites of older eruptions from literature (Cristofolini *et al.*, 1981; D'Orazio *et al.*, 1998), in order to constrain the chemical and physical conditions of the different crystallizing systems.

2. Mineralogy and petrography of 2001 lavas and tephra

Amphibole was found both in lavas and tephra erupted during the 2001 eruption at Mount Etna, which was characterized by the opening of several eruptive fissures on the southern flank of the volcano from the base of the SE crater down to the Mts. Calcarazzi area (3100−2100 m a.s.l.). An amphibole-bearing trachybasaltic magma was erupted from vents located along N-S trending fractures (2100−2550 m a.s.l.), whereas a different trachybasaltic magma, with no amphibole, was erupted through NNW-SSE trending structures (3100−2600 m a.s.l.) (*cf.* Clocchiatti *et al.,* 2004; Metrich *et al.,* 2004; Monaco *et al.,* 2005; Viccaro *et al*., 2006; Corsaro *et al.,* 2007). Two distinct vent systems were active approximately at the lower and higher ends of the N-S fractures, at the Mts. Calcarazzi and Laghetto areas respectively.

The amphibole-bearing lavas are generally mesophyric (P.I. ∼20 %) with a seriate texture. Their phenocryst assemblage is mainly composed of calcic plagioclase (bytownite to labradorite) and augitic clinopyroxene in similar proportions, with olivine (Fo_{70-79}) and Ti-magnetite as minor phases. Augite and plagioclase are generally euhedral with their sizes attaining up to ∼ 1 cm. Olivine and Ti-magnetite are from subhedral to euhedral, reaching the maximum sizes of about 100−200 μm. The groundmass is hyaline to microcrystalline, generally intersertal to hyalopilitic with a poorly developed fluidal texture. The microlites are mainly plagioclase, scarce clinopyroxene and olivine, with Ti-magnetite and apatite as minor phases.

Tephra are lapilli and shards due to the fragmentation of the magma foam, and are composed with euhedral clinopyroxene phenocrysts, phenoclasts (up to 1 cm) and micro-phenocrysts of plagioclase, whereas olivine and Ti-magnetite are scarce. Crystals are generally enclosed in an abundant glassy groundmass, highly vesicular with bubble volume always > 50 %, as expected by fragmentation related to expansion of juvenile gas in an uprising magma (Fisher & Schmincke, 1984; 1994). Glass varies from pale yellow sideromelane to deep orange-brown tachylyte, probably as a consequence of an increasing degree of hydrothermal transformation by fumarole vapours. Patches of limpid and clear sideromelane with rare plagioclase microlites commonly occur in fine-grained clasts, that were quenched fast and efficiently enough to prevent a massive nucleation of opaque phases. Sideromelane is most abundant in tephra related to the final phase of the eruptive activity (*cf.* Taddeucci *et al.*, 2004).

Amphibole is about 2−3 vol.% in lavas and scarcer in tephra; it is generally found as isolated euhedral to subhedral phenocrysts (Fig. 1a, b) and sometimes as megacrysts up to 10 cm along the *c* axis. Larger phenocrysts (> 1−2 cm) are frequently poikilitic and enclose plagioclase, augite and scarcer olivine (Fig. 1c). Crystals optically resemble the Etnean amphiboles of prehistoric lavas (Klerkx, 1964; 1968; Cristofolini & Lo Giudice, 1969; Tanguy, 1980; Cristofolini *et al.*, 1981), as they are characteristically cleaved according to {110}, markedly pleocroic (α = brown – light brown; $\beta \cong \gamma$ = reddish-brown to intense brown), and with $z\hat{}\gamma < 5°$. Amphibole phenocrysts found in lavas are always jacketed by a microvesicular cryptocrystalline reaction rim, likely evidence of a syn-eruptive instability (Fig. 1b). These rims are about 0.5 mm wide in the largest phenocrysts, and are made of a mixture of fassaïte, rhönite and anorthite with interstitial K-rich residual glass (Clocchiatti & Tanguy, 2001; Clocchiatti *et al.*, 2004; Lopez *et al.*, 2006). Phenocrysts with no reaction rims exclusively occur in tephra (Fig. 1d), suggesting that, due to melt quenching, the original equilibrium between the crystals and the melt was preserved.

3. Analytical techniques

Several amphibole phenocrysts have been selected from lavas and tephra for mineral-chemical characterization. However, only five of them, found in tephra grains, display the surrounding glass at equilibrium, so that amphibole/melt partition coefficients for REE and trace elements have been exclusively calculated for these five pairs. Compositions at the rim of amphibole crystals and of the glass at their edges were selected as representing conditions as close as possible to solid/melt thermodynamic equilibrium. Major element contents of amphibole and glass (Tables 1 and 2) were analysed by means of a CAMECA SX50 electron microprobe (EMP) equipped

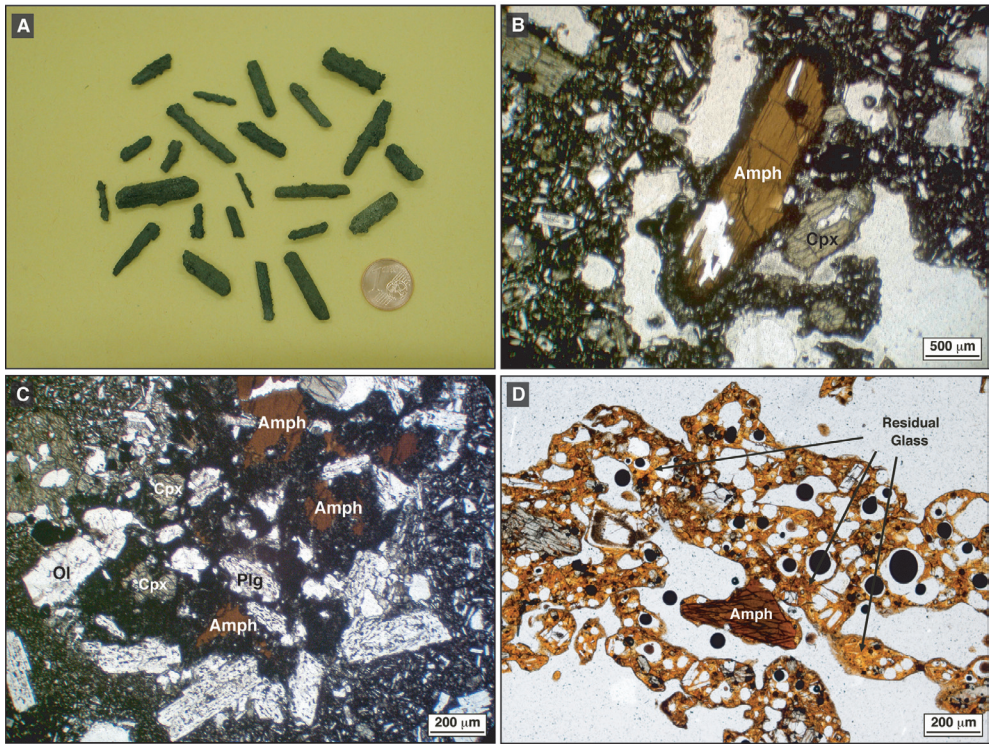

Fig. 1. A) Isolated euhedral megacrysts of Mg-hastingsite, 2–3 cm long, sampled from the earlier erupted products of the 2001 eruption at the 2100 m vent near the Mts. Calcarazzi area. B) Subhedral Mg-hastingsite crystal showing a characteristic cryptocrystalline reaction rim; // polars. C) Poikilitic structure of a strongly resorbed Mg-hastingsite (as relics) megacryst, with enclosed phenocrysts of plagioclase, clinopyroxene and olivine; // polars. D) Selected tephra of the 2001 eruption at Mt. Etna; a Mg-hastingsite crystal is clearly visible with other phases constituted by phenocrysts and microphenocrysts of clinopyroxene and plagioclase. All phases are in equilibrium with the surrounding highly vesiculated sideromelane (bubbles > 50 vol.%); // polars.

with four WDS spectrometers at the CNR-IGG, Unit of Padova. Operating conditions were set at 15 keV accelerating potential, 15 nA beam current and peak counting times of 15 s. The analytical precision is better than 1 % for SiO_2, Al_2O_3, FeO, MgO and CaO and better than 3 % for TiO_2, Cr_2O_3, MnO, Na_2O, K_2O and P_2O_5. Minor and trace element concentrations of the five selected amphibole/glass pairs (Table 3) were analysed by means of Laser Ablation Microprobe Inductively Coupled Plasma Mass Spectrometry (LAM-ICP/MS) at the CNR-IGG, Unit of Pavia. The basic setup of the instrument is carefully described in Bottazzi *et al.* (1999), with the most important change consisting in the adoption of a shorter laser wavelength (213 nm), resulting from mixing of the fundamental radiation (1064 nm) with the fourth harmonic radiation (266 nm) into a third harmonic generator (Jeffries *et al.,* 1998). The analytical precision of this LAM-ICP/MS is given better than 7 % for all the analysed trace elements (see www_crystal.unipv.it/precision_and_accuracy.htm).

4. Chemistry of amphibole and glass

4.1 Amphibole

The structural formulae of the analysed crystals were calculated on the basis of 13 cations and 23 oxygen atoms with Fe^{2+}/Fe^{3+} recalculation, as recommended by Leake *et al.* (1978). Data are compared with major element contents and structural formulae for phenocrysts of kaersutite referred to prehistoric products with hawaiitic to trachytic compositions (Cristofolini *et al*., 1981; D'Orazio *et al*., 1998). According to the Leake *et al.* (1997) nomenclature for Ca-amphiboles, the analysed amphibole crystals from the 2001 lavas and tephra are *titanian Mg-hastingsites* and very rarely *titanian pargasites*.

The Mg-hastingsite chemically differs from the amphiboles of prehistoric eruptions mainly for its generally lower proportions of Ti and higher ones of Al^{VI}, Ca and especially K; significant differences also occur for Fe_{tot} (data source for prehistoric amphiboles Cristofolini *et al.*, 1981; D'Orazio *et al.*, 1998):

	Ti	Al^{VI}	Fe^{3+}	Fe^{2+}	Ca	K
Mg-hast: aver. (21 analyses)	0.399	0.267	0.381	0.945	1.927	0.189
σ	(0.02)	(0.04)	(0.09)	(0.10)	(0.02)	(0.02)
Kaers – Parg: aver. (6 analyses)	0.537	0.218	n.d.	1.385	1.801	0.153

Al^{IV} values (aver. 2.137 a.f.u.) are generally higher, with rare exceptions, than those of kaersutite and titanian pargasite of older lavas (aver. 2.016 a.f.u.) (Fig. 2). Finally, the Mg# values [$Mg/(Mg + Fe^{2+})$] in Mg-hastingsite of the 2001 eruption (0.71–0.80) are higher than in prehistoric

Table 1. Major oxide compositions (wt.%) and structural formulae for the analysed amphibole phenocrysts.

Sample	Am1-A1	Am1-A2	Am1-A3	Am1-A4	Am2-A1	Am2-A2	Am2-A3	Am2-A4	Am3-A1	Am3-A2	Am4-A1	Am4-A2	Am7-A1	Am8-A1	Am8-A2	Am9-A1	Am9-A2	Am6-A1	Am6-A2	Am5-A1	Am5-A2
Classif	Mg-hast	Mg-hast	Mg-hast	Mg-hast	Mg-hast	Mg-hast	Mg-hast	Mg-hast	Mg-hast	Mg-hast	Mg-hast	Mg-hast	Mg-hast	Mg-hast	Parg	Parg	Mg-hast	Mg-hast	Mg-hast	Mg-hast	Mg-hast
Modifiers	Titanian	Titanian	Titanian	Titanian	Titanian	Titanian	Titanian	Titanian	Titanian	Titanian	Titanian	Titanian	Titanian	Titanian	Titanian	Titanian	Titanian	Titanian	Titanian	Titanian	Titanian
SiO_2	40.0	40.3	40.0	40.2	39.8	39.8	40.0	39.6	39.8	40.3	39.9	39.5	40.0	39.8	40.1	40.9	41.4	40.9	40.3	40.0	40.3
TiO_2	3.62	3.59	3.77	3.61	3.54	3.72	3.66	3.48	3.52	3.72	3.74	3.85	3.62	3.58	3.59	3.64	4.15	3.79	3.34	3.49	3.54
Al_2O_3	14.0	14.1	14.2	13.9	14.2	14.4	14.3	14.2	14.2	14.4	14.2	14.4	13.5	13.9	14.1	13.0	12.2	13.7	14.2	14.4	14.3
Cr_2O_3	0.03	n.d.	0.06	0.05	n.d.	0.04	n.d.	0.01	0.04	0.02	0.02	n.d.	n.d.	0.04	n.d.	n.d.	0.01	0.01	n.d.	0.09	n.d.
FeO	11.1	11.1	10.5	11.1	11.0	11.6	11.6	11.4	10.5	11.0	10.7	10.6	11.6	10.5	10.4	10.8	11.3	10.4	10.4	10.3	10.3
MnO	0.13	0.14	0.21	0.19	0.07	0.16	0.08	0.16	0.09	0.14	0.12	0.08	0.06	0.13	0.03	0.19	0.11	0.12	0.11	0.11	0.15
MgO	13.6	13.9	13.6	13.9	13.7	13.3	13.3	13.5	13.8	13.6	13.8	13.8	13.4	14.2	13.6	13.8	13.7	14.1	14.1	14.2	14.1
CaO	12.4	12.3	12.1	12.5	12.3	12.4	12.3	12.2	12.4	12.4	12.4	12.4	12.3	12.4	12.4	12.3	11.9	12.1	12.2	12.4	12.5
Na_2O	2.29	2.39	2.35	2.29	2.31	2.11	2.24	2.24	2.20	2.16	2.20	2.26	2.30	2.26	2.19	2.44	2.45	2.32	2.35	2.09	2.22
K_2O	1.07	1.06	1.10	1.02	1.08	0.99	1.09	1.08	1.10	1.00	1.05	1.15	0.88	1.02	1.12	0.98	0.74	0.72	0.80	1.10	1.15
Total	98.2	98.9	97.9	98.7	98.0	98.6	98.5	97.9	97.7	98.7	98.1	98.1	97.7	97.9	97.5	98.0	98.1	98.2	97.8	98.1	98.5
Si	5.847	5.842	5.859	5.851	5.822	5.795	5.827	5.806	5.832	5.842	5.830	5.780	5.880	5.808	5.897	6.001	6.057	5.916	5.864	5.813	5.846
Al^{IV}	2.153	2.158	2.141	2.149	2.178	2.205	2.173	2.194	2.168	2.158	2.170	2.220	2.120	2.192	2.103	1.999	1.943	2.084	2.136	2.187	2.154
∑Z	8.000	8.000	8.000	8.000	8.000	8.000	8.000	8.000	8.000	8.000	8.000	8.000	8.000	8.000	8.000	8.000	8.000	8.000	8.000	8.000	8.000
Ti	0.399	0.392	0.415	0.394	0.390	0.407	0.402	0.384	0.388	0.406	0.411	0.423	0.400	0.393	0.397	0.401	0.456	0.413	0.366	0.381	0.386
Al^{VI}	0.266	0.253	0.302	0.226	0.272	0.263	0.281	0.256	0.290	0.304	0.273	0.256	0.218	0.205	0.335	0.239	0.159	0.258	0.293	0.279	0.289
Cr	0.003	0.000	0.007	0.005	0.000	0.005	0.000	0.001	0.005	0.002	0.003	0.000	0.000	0.005	0.000	0.000	0.001	0.001	0.000	0.011	0.000
Fe^{3+}	0.350	0.428	0.328	0.405	0.400	0.483	0.415	0.508	0.369	0.386	0.393	0.391	0.412	0.478	0.229	0.219	0.302	0.465	0.481	0.483	0.377
Fe^{2+}	1.009	0.915	0.961	0.944	0.947	0.931	0.994	0.886	0.914	0.950	0.909	0.906	1.018	0.809	1.045	1.105	1.081	0.800	0.788	0.763	0.876
Mn	0.016	0.017	0.025	0.023	0.009	0.019	0.010	0.020	0.011	0.017	0.015	0.010	0.008	0.016	0.004	0.024	0.013	0.015	0.014	0.013	0.019
Mg	2.957	2.995	2.961	3.001	2.983	2.892	2.899	2.944	3.023	2.935	2.998	3.015	2.944	3.094	2.991	3.011	2.988	3.049	3.057	3.071	3.053
∑X	5.000	5.000	5.000	5.000	5.000	5.000	5.000	5.000	5.000	5.000	5.000	5.000	5.000	5.000	5.000	5.000	5.000	5.000	5.000	5.000	5.000
Ca	1.943	1.913	1.901	1.944	1.935	1.931	1.920	1.912	1.949	1.930	1.931	1.937	1.934	1.944	1.955	1.931	1.869	1.875	1.909	1.930	1.938
Na	0.650	0.672	0.666	0.647	0.655	0.596	0.632	0.637	0.625	0.608	0.622	0.639	0.656	0.639	0.625	0.693	0.693	0.651	0.664	0.588	0.626
K	0.199	0.196	0.205	0.188	0.202	0.183	0.202	0.201	0.205	0.186	0.195	0.214	0.165	0.190	0.210	0.184	0.138	0.133	0.148	0.205	0.214
∑Y	2.793	2.781	2.773	2.779	2.792	2.710	2.754	2.750	2.780	2.724	2.749	2.790	2.756	2.774	2.790	2.808	2.700	2.659	2.720	2.723	2.778
∑X+Y+Z	15.793	15.781	15.773	15.779	15.792	15.710	15.754	15.750	15.780	15.724	15.749	15.790	15.756	15.774	15.790	15.808	15.700	15.659	15.720	15.723	15.778
Mg#	0.75	0.77	0.75	0.76	0.76	0.76	0.74	0.77	0.77	0.76	0.77	0.77	0.74	0.79	0.74	0.73	0.73	0.79	0.79	0.80	0.78

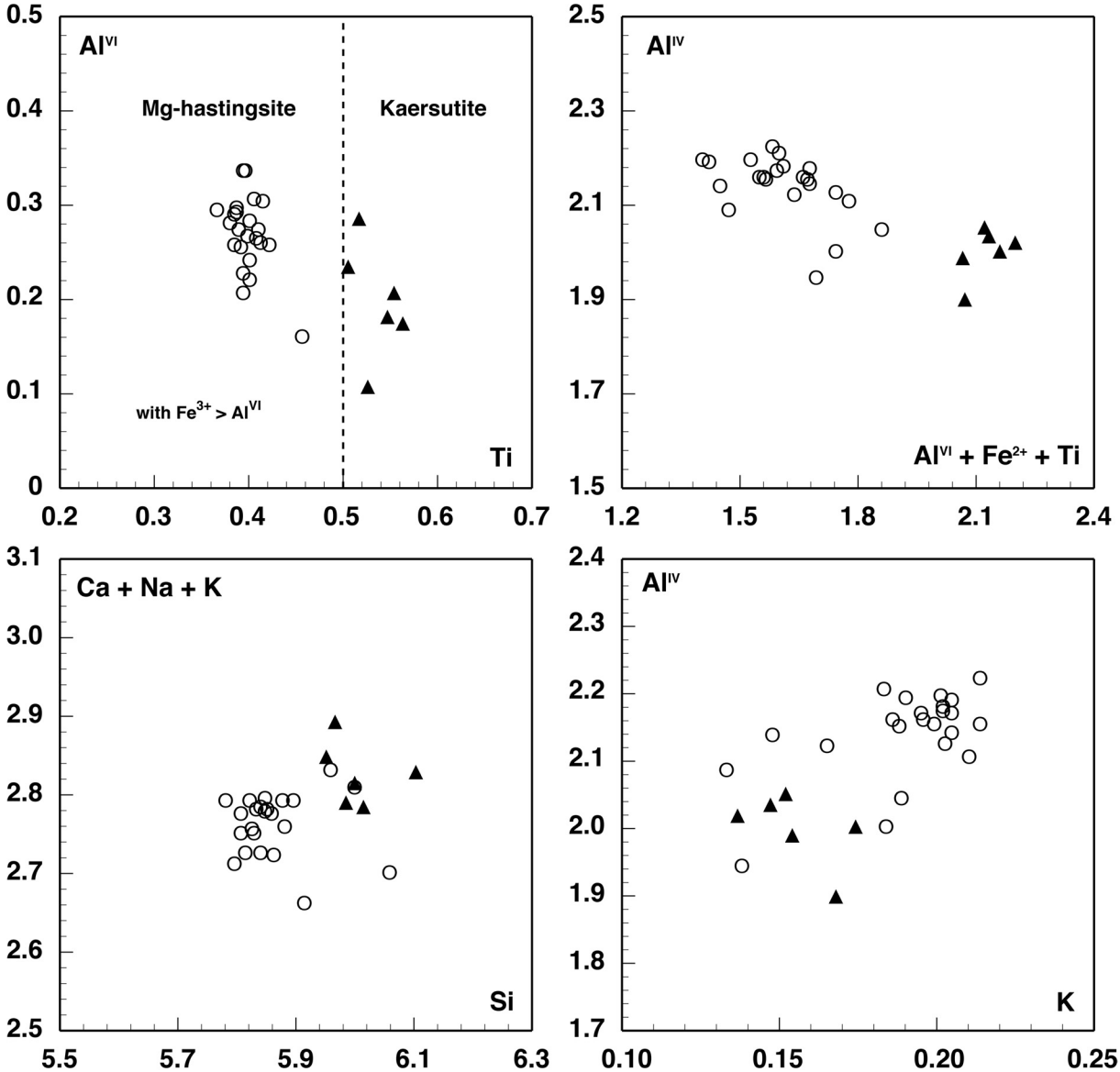

Fig. 2. Cations per formula unit (a.f.u.) for phenocrysts of Mg-hastingsite of the 2001 event (circles) and the prehistoric kaersutite (triangles; Cristofolini *et al.*, 1981; D'Orazio *et al.*, 1998). Mg-hastingsite especially differs from kaersutite for its higher values of Al^{IV}, Al^{VI} and K.

Table 2. Major element concentrations (wt.%) for the analysed glasses found in tephra fragments.

Sample	1 GL01	2 GL01	3 GL01	4 GL01	5 GL01	6 GL01	7 GL01	8 GL01	9 GL01	10 GL01
SiO_2	50.1	51.0	51.0	50.9	51.0	50.9	51.0	51.1	51.2	50.8
TiO_2	2.13	1.96	1.91	2.13	2.02	1.99	2.01	1.97	2.00	1.98
Al_2O_3	16.1	16.5	16.6	16.7	16.6	16.4	16.6	16.7	16.6	16.8
FeO	10.9	10.7	10.7	10.5	10.6	10.8	10.9	10.5	10.5	10.5
MgO	3.35	3.31	3.27	3.24	3.26	3.20	3.22	3.22	3.07	3.29
MnO	0.23	0.21	0.14	0.20	0.16	0.26	0.15	0.18	0.20	0.16
CaO	7.04	7.53	7.46	7.44	7.50	7.45	7.45	7.35	7.44	7.50
Na_2O	4.19	4.20	4.32	4.22	4.25	4.36	3.99	4.30	4.32	4.36
K_2O	2.97	3.34	3.52	3.56	3.40	3.50	3.49	3.52	3.66	3.49
P_2O_5	1.14	1.05	0.82	0.95	0.97	0.91	0.90	0.93	0.91	0.91
Total	98.2	99.8	99.7	99.8	99.8	99.8	99.7	99.8	99.9	99.8

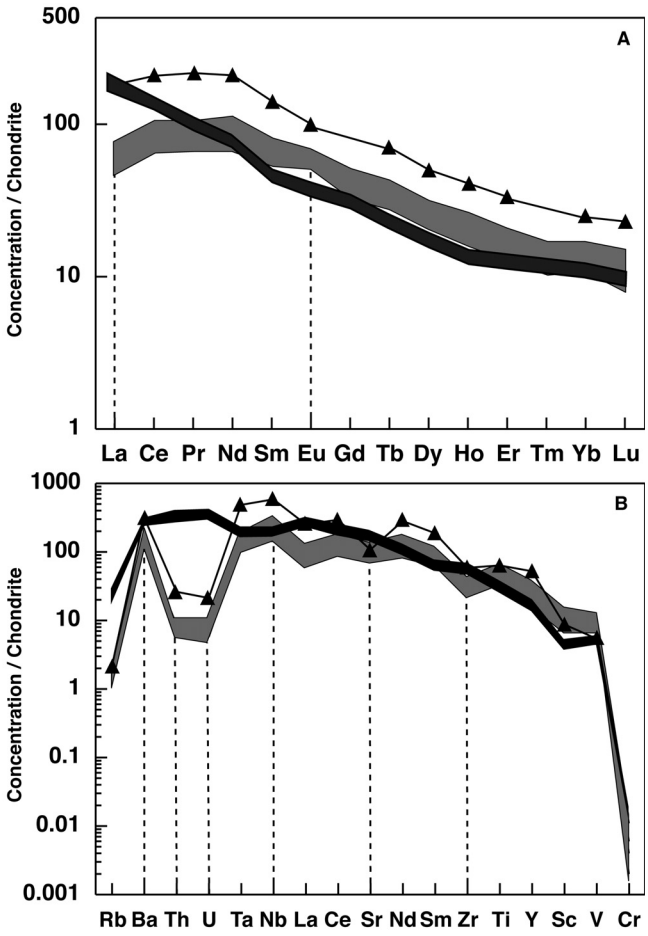

Fig. 3. Chondrite-normalized patterns for the Mg-hastingsite phenocrysts of the 2001 eruption (grey field) and the prehistoric kaersutite (triangles; D'Orazio *et al.*, 1998); patterns of residual glasses found in tephra fragments (black field) are also shown for comparison. A) REE patterns (Sun, 1982); B) incompatible and compatible trace elements (Sun & McDonough, 1989; and Anders & Ebihara, 1982).

amphiboles (0.67–0.69; Cristofolini *et al.*, 1981; D'Orazio *et al.*, 1998).

The Chondrite-normalized (Sun, 1982) REE patterns are rather homogeneous for all of the analysed Mg-hastingsite phenocrysts (Fig. 3a), with a negative La anomaly. La_N/Sm_N (0.92–1.09) and La_N/Yb_N (4.39–5.31) are consequently lower than Ce_N/Sm_N (5.46–6.20) and Ce_N/Yb_N (24.34–28.18). On the whole LREE are generally notably enriched, whereas MREE and HREE are fractionated (Sm_N/Yb_N = 4.56–5.12). A slightly positive Eu anomaly occurs (Eu/Eu* between 1.06 and 1.26). The Chondrite-normalized (Sun, 1982) REE pattern for a kaersutite of the Ellittico volcanic sequence (D'Orazio *et al.*, 1998) is shown for comparison (Fig. 3a). This pattern displays concentrations markedly higher than in Mg-hastingsite for all of the REE, but LREE/HREE ratios (La_N/Sm_N = 1.32; La_N/Yb_N = 7.49; Sm_N/Yb_N = 5.67) are similar. La is slightly depleted, whereas no Eu anomaly is apparent.

The Chondrite-normalized (Sun & McDonough, 1989; and Anders & Ebihara, 1982) extended patterns for incompatible and compatible trace elements of Mg-hastingsite are rather homogeneous (Fig. 3b) and show clear anomalies, negative for Th, U, Zr, and positive for Ba and Nb. The extended pattern of kaersutite from prehistoric lavas (D'Orazio *et al.*, 1998) is similar to that of Mg-hastingsite, but with higher concentrations for most of the trace elements. Sr is, however, less enriched and shows a pronounced negative anomaly, as well as the transition elements, which are slightly less abundant than in Mg-hastingsite.

4.2 Glass

The analysed sideromelane patches are basaltic-trachyandesite in composition (Le Maitre, 2002), at the boundary with the trachybasaltic and phono-tephritic fields, well within the range observed by Taddeucci *et al.* (2004) for glasses sampled from distinct vents of the 2001 eruption. As expected, the residual glass is more concentrated in TiO_2, Na_2O, K_2O and P_2O_5 compared to the whole rock compositions (*cf.* Clocchiatti *et al.,* 2004; Metrich *et al.,* 2004; Viccaro *et al.,* 2006; Corsaro *et al.*, 2007). MgO and CaO values are instead lower in the residual glass than in the bulk rock, whereas the Al_2O_3 content does not significantly differ.

The Chondrite-normalized patterns for REE (Sun, 1982) and trace elements (Sun & McDonough, 1989; and Anders & Ebihara, 1982) of residual glass are shown in Fig. 3a, b. Compared with Mg-hastingsite, they display higher concentrations of La, Ce, LILE, Th, U and lower concentrations of Ti, Y, Sc, V. On the whole, all of the trace element concentrations in the glass are similar to those analysed in groundmasses of hawaiites referred to a prehistoric Etnean volcanic centre (Ellittico) by D'Orazio *et al.* (1998).

5. Discussion

5.1 Amphibole/melt trace element partitioning

Partition coefficients ($^{Amph/melt}D$) for REE + Y, LILE, HFSE and transition elements for five selected amphibole/melt pairs were calculated as the mass ratio between the concentration of the *i* element in the solid phase (the amphibole rim) and in the coexisting melt (the surrounding glass) (Table 3).

$^{Amph/melt}D$ are lower for LREE and higher for MREE and HREE (Fig. 4a). Among REE, partition coefficients of La, Ce and Pr are the only ones with values < 1, whereas they are > 1.1 from Nd to Lu, with the highest value reached by Ho and with peaks also for Eu and Tb. Slightly lower $^{Amph/melt}D$ are observed for Y and HREE.

The partition coefficients of some LILE and HFSE are $\ll 1$, with the exception of Nb. Rb, U and Th show the lowest $^{Amph/melt}D$ (Fig. 4b; Table 3). For other LILE and HFSE (Ba, Sr, Ta, Zr and Hf) the values are generally < 1. Among them, Nb appears as the most compatible.

Table 3. Trace element concentrations (ppm) for the analysed amphibole phenocrysts and glasses in tephra. The analytical precision is given better than 7 % for all the analysed elements (www_crystal.unipv.it/precision_and_accuracy.htm). Partition coefficients ($^{Amph/melt}D$) have been calculated for each amphibole/melt pair and averaged values with the σ have been also reported.

Sample	Am1-A3 2 GL01		$^{Amph/melt}D$	Am2-A4 4 GL01		$^{Amph/melt}D$	Am4-A2 8 GL01		$^{Amph/melt}D$	Am7-A1 6 GL01		$^{Amph/melt}D$	Am9-A1 1 GL01		$^{Amph/melt}D$	$^{Amph/melt}D$	σ
																Average	
Li	21	n.d.	n.d.	26	n.d.	n.d.	20	n.d.	n.d.	27	n.d.	n.d.	24	n.d.	n.d.	**n.d.**	**n.d.**
Cs	n.d.	n.d.	n.d.	n.d.	n.d.	n.d.	n.d.	n.d.	n.d.	0.03	n.d.	n.d.	n.d.	n.d.	n.d.	**n.d.**	**n.d.**
Rb	3.2	48.9	0.065	3.0	48.2	0.062	3.1	50.3	0.062	3.0	47.8	0.063	3.0	47.3	0.063	**0.063**	**±0.001**
Ba	391	637	0.614	331	584	0.567	324	614	0.528	315	582	0.541	340	596	0.570	**0.564**	**±0.033**
Th	0.23	9.2	0.025	0.23	9.2	0.025	0.25	9.3	0.027	0.21	9.2	0.023	0.21	9.1	0.023	**0.025**	**±0.002**
U	0.048	2.62	0.018	0.065	2.82	0.023	0.046	2.51	0.018	0.048	2.56	0.019	0.054	2.59	0.021	**0.020**	**±0.002**
Nb	44	35	1.257	52	43	1.209	46	38	1.211	62	51	1.216	55	45	1.222	**1.223**	**±0.020**
Ta	1.7	2.5	0.680	2.0	2.9	0.690	1.8	2.7	0.667	2.1	3.0	0.700	1.8	2.6	0.692	**0.686**	**±0.013**
Pb	0.66	n.d.	n.d.	0.67	n.d.	n.d.	0.58	n.d.	n.d.	0.64	n.d.	n.d.	0.66	n.d.	n.d.	**n.d.**	**n.d.**
Sr	699	1315	0.532	691	1340	0.516	641	1250	0.513	738	1380	0.535	605	1190	0.508	**0.521**	**±0.012**
Zr	102	178	0.573	113	195	0.579	112	192	0.583	126	211	0.597	115	196	0.587	**0.584**	**±0.009**
Hf	3.6	4.2	0.857	4.1	4.7	0.872	4.0	4.7	0.851	4.5	5.1	0.882	4.1	4.8	0.854	**0.863**	**±0.013**
La	20.8	57.1	0.364	22.2	59.6	0.372	16.8	47.1	0.357	22.6	61.5	0.367	22.5	60.8	0.370	**0.366**	**±0.006**
Ce	74.4	110	0.676	77.1	113	0.682	62.8	101	0.622	79.1	115	0.688	81.3	118	0.689	**0.671**	**±0.028**
Pr	10.8	11.3	0.956	11.3	11.9	0.950	9.6	10.0	0.960	11.9	12.3	0.967	12.2	12.7	0.961	**0.959**	**±0.007**
Nd	52.5	43.2	1.215	54.8	44.9	1.220	46.5	39.3	1.183	60.2	48.5	1.241	61.7	47.9	1.288	**1.230**	**±0.039**
Sm	12.0	7.9	1.519	13.1	8.4	1.560	11.5	7.5	1.533	14.1	9.1	1.549	14.4	9.4	1.532	**1.539**	**±0.016**
Eu	4.3	2.63	1.635	4.4	2.68	1.642	4.5	2.73	1.648	4.7	2.84	1.655	4.7	2.85	1.649	**1.646**	**±0.008**
Gd	10.1	7.61	1.327	10.9	8.15	1.337	10.0	7.49	1.335	12.6	9.37	1.345	11.2	8.35	1.341	**1.337**	**±0.007**
Tb	1.55	0.99	1.566	1.72	1.07	1.607	1.50	0.94	1.596	1.90	1.17	1.624	1.82	1.13	1.611	**1.601**	**±0.022**
Dy	7.7	5.19	1.484	8.8	5.91	1.489	7.9	5.27	1.499	9.5	6.35	1.496	8.8	5.89	1.494	**1.492**	**±0.006**
Ho	1.37	0.84	1.631	1.61	0.94	1.713	1.34	0.81	1.654	1.82	1.08	1.685	1.73	1.02	1.696	**1.676**	**±0.033**
Y	34	22.7	1.498	36	24.2	1.488	32	21.3	1.502	45	29.8	1.510	37	24.8	1.492	**1.498**	**±0.009**
Er	3.1	2.45	1.265	3.5	2.74	1.277	3.1	2.41	1.286	4.2	3.26	1.288	3.6	2.81	1.281	**1.280**	**±0.009**
Tm	0.40	n.d.	n.d.	0.46	n.d.	n.d.	0.40	n.d.	n.d.	0.52	n.d.	n.d.	0.50	n.d.	n.d.	**n.d.**	**n.d.**
Yb	2.64	2.1	1.257	2.96	2.4	1.233	2.58	2.1	1.229	3.30	2.6	1.269	3.00	2.4	1.250	**1.248**	**±0.017**
Lu	0.30	0.24	1.250	0.37	0.29	1.276	0.40	0.32	1.250	0.45	0.35	1.286	0.42	0.33	1.273	**1.267**	**±0.016**
Sc	61	27	2.259	46	21	2.190	69	32	2.156	59	26	2.269	55	24	2.292	**2.233**	**±0.057**
V	484	237	2.042	452	219	2.064	521	251	2.076	450	215	2.093	550	268	2.052	**2.065**	**±0.020**
Cr	4	17	0.235	10	29	0.345	0.38	2	0.190	29	47	0.617	16	36	0.444	**0.366**	**±0.172**
Co	59	28	2.107	64	31	2.065	62	30	2.067	62	29	2.138	67	32	2.094	**2.094**	**±0.030**

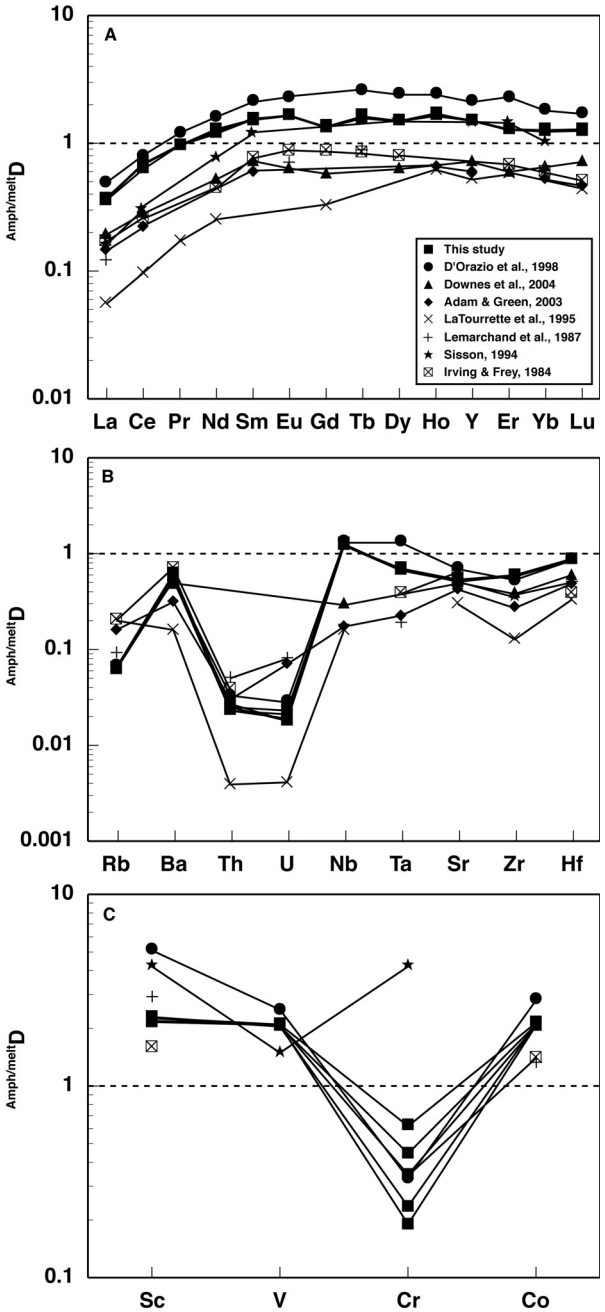

Fig. 4. Calculated partition coefficients ($^{Amph/melt}D$) between the Mg-hastingsite phenocrysts of the 2001 eruption and the coexisting residual glasses for A) REE, B) LILE and HFSE, C) transition elements. $^{Amph/melt}D$ measured in this study have been compared with previous results from literature data (Irving & Frey, 1984; Lemarchand *et al.*, 1987; Sisson, 1994; LaTourrette *et al.*, 1995; D'Orazio *et al.*, 1998; Adam & Green, 2003; Downes *et al.*, 2004).

Partition coefficients for the transition elements are > 2, except for Cr that shows $^{Amph/melt}D$ lower than 1 (Fig. 4c; Table 3). Sc shows the largest value, whereas the values for Co and V are slightly lower.

Several attempts have been carried out by many authors in order to define $^{Amph/melt}D$ values for basic melts at various experimental P and T conditions (Higuchi & Nagasawa, 1969; Irving & Frey, 1984; Green & Pearson, 1985; Lemarchand *et al.,* 1987; Adam & Green, 1994; 2003; Sisson, 1994; LaTourrette *et al.,* 1995; D'Orazio *et al.,* 1998; Tiepolo *et al.,* 2000; 2001; Downes *et al.,* 2004). A comparison can be made between $^{Amph/melt}D$ obtained in this work and those obtained from literature, related to the trace element partitioning between amphibole and basaltic/alkali basaltic melts (Fig. 4). $^{Amph/melt}D$ values of Mg-hastingsite of the 2001 eruption display patterns similar to those reported in literature for REE, HFSE and transition elements, related to other amphiboles and melts (*cf.* Irving & Frey, 1984; Lemarchand *et al.,* 1987; Adam & Green, 2003; Sisson, 1994; LaTourrette *et al.,* 1995; Downes *et al.,* 2004). In detail, $^{Amph/melt}D$ values of the Etnean Mg-hastingsite are higher than those from the above cited references for REE, Nb, Ta, Zr and Hf, and much lower for Rb, Th, and U. Partitioning of other elements is instead similar for the whole data set.

More interestingly, the comparison between $^{Amph/melt}D$ for Mg-hastingsite and those of a kaersutite, crystallized from a benmoreitic Etnean melt (D'Orazio *et al.*, 1998), shows that these amphiboles display rather similar patterns for all of the trace elements, although Mg-hastingsite values are significantly lower for most of the elements than the ones reported for kaersutite (Fig. 4). This tendency is quite clear for REE and Sc, and to a minor extent for Th, U, Ta, Sr, V and Co.

Reasons of this difference are to be found by taking into account that trace element partitioning between amphibole and melt depends on several factors among which the most important ones are the compositions of the coexisting minerals and/or of the hosting melt (Pearce & Norry, 1979; Mysen & Virgo, 1980; Nicholls & Harris, 1980; Green & Pearson, 1985; Lemarchand *et al.*, 1987; Sisson, 1994). Other factors, however, such as temperature (Nicholls & Harris, 1980; Green & Pearson, 1985), pressure (Green & Pearson, 1985; Adam & Green, 1994; 2003) and fO_2 (Green & Pearson, 1985) may have major effects on partition coefficients. Experimental studies on amphiboles in basaltic and andesitic systems demonstrated that $^{Amph/melt}D$ values for REE and other trace elements are positively correlated with the SiO_2 content of the melt (Lemarchand *et al.*, 1987; Sisson, 1994), and negatively correlated with the temperature of the melt (Green & Pearson, 1985). Green & Pearson (1985) established that $^{Amph/melt}D_{REE}$ values slightly decrease with increasing fO_2 and total pressure. A similar behaviour was also found for Ti and REE partition coefficients in amphiboles under equilibrium with basanitic melts by Adam & Green (1994; 2003). Anyhow, these authors suggest that different fO_2 conditions as well as addition of H_2O to the system do not significantly affect the partition coefficients.

5.2 Effects of amphibole fractionation

Many authors have suggested that pargasitic-kaersutitic-Mg-hastingsitic amphiboles exert a significant role in the petrogenesis of alkali basaltic rocks, at first as possible

accessory phases during the partial melting process in the source region and later when magmas differentiate by crystal fractionation (Aoki, 1963; Baker, 1969; Gast, 1968; Griffin & Murthy, 1969; Le Maitre, 1962; 1969; Kesson & Price, 1972). The partitioning between Mg-hastingsite and melt discussed above points out some possible implications that the amphibole crystallization may exert in modifying the geochemical features of magmas stored in reservoirs of active volcanoes. In detail, Th, U and LREE can be incorporated in much lower amounts compared to other trace elements such as Nb and Ta. This means that, if Mg-hastingsite fractionation occurs, the trace element signature of residual melts might be strongly affected, due to increased ratios of trace elements, like U/Nb, Th/Ta, La/Nb, La/Ta. Through the careful geochemical analysis of products of the 2001 eruption it is possible to test the efficacy of amphibole growth in controlling these petrologically important ratios. Specifically, several authors have given evidence that two distinct magmas were simultaneously erupted from two fracture systems on the southern flank of the volcano (Clocchiatti *et al.,* 2004; Metrich *et al.,* 2004; Viccaro *et al.,* 2006; Corsaro *et al.,* 2007): an amphibole-bearing trachybasaltic magma from N-S trending fractures (2550−2550 m), and a trachybasaltic magma, with no amphibole at all, from NNW-SSE trending ones (3100−2600 m). Averaged geochemical data on glasses in tephra from the two distinct systems show that ratios such as Th (or U)/Ta and, to a minor extent, Th/Nb and La/Nb are higher in the amphibole-bearing products than in those where amphibole is absent (data source Viccaro, 2006; *cf.* Viccaro *et al.,* 2006; Corsaro *et al.,* 2007). The amphibole growth is also fundamental in controlling the overall melt composition. Clues to investigate this relationship can be found by examining the behaviour of $^{Amph/melt}D_{Nb/Zr}$, as stated by Tiepolo *et al.,* (2000; 2001). They remarked that the Nb/Zr ratio in the melt is positively related to the Mg# of the amphibole, mainly due to effects induced by amphibole and melt structure (*e.g.* crystal structure, degree of polymerization). The comparison between the Mg-hastingsite from the 2001 eruption and the kaersutite from prehistoric eruptions offers the opportunity to verify this statement. Even considering the rather distinct melt compositions from which Mg-hastingsite and kaersutite crystallized (basaltic-trachyandesite and benmoreite respectively), Mg# is much higher in Mg-hastingsite than in kaersutite (Cristofolini *et al.,* 1981; D'Orazio *et al.,* 1998). The averaged $^{Amph/melt}D_{Nb/Zr}$ value turns to be 1.99 for Mg-hastingsite (Table 3), whereas it is 2.45 for kaersutite (*cf.* D'Orazio *et al.,* 1998). The resulting Nb/Zr ratio is then almost twice as much in the basaltic-trachyandesite residual melt compared to that in the benmoreite (0.45 *vs.* 0.26). Issues of a much broader interest could rise from the specific instance supplied by the amphibole crystallization at depth in the Etnean feeding system, if one considers that it may play a significant role in controlling the HFSE and LREE signature of magmas coming also from feeding systems of other alkali basaltic volcanoes (*e.g.* Hawaii, St. Helena, Gough Island, Tristan da Cunha). This feature becomes of great importance especially for these systems, where amphibole is an uncommonly found phase, and consequently its possible role in the magma system could be defined by anomalies affecting trace element ratios in the melts.

5.3 Constraints on Mg-hastingsite crystallization

Integrated petrological and geophysical data related to the 2001 eruption at Mt. Etna constrain at ~ 200 MPa the lowest pressure value needed to crystallize Mg-hastingsite (Viccaro *et al.*, 2006 and references therein). At this pressure, an equilibrium T of ~ 980 °C for Mg-hastingsite can be deduced from phase equilibria and experimental results (Deer *et al.*, 1997 and references therein). Comparable results (T ~ 970 °C) have been obtained using the geothermometer proposed by Otten (1984), calibrated on the Ti content of hornblende under QFM buffered fO_2 conditions. Such a T is however slightly underestimated. A reason can be found by considering that coexisting magnetite-ilmentite are needed for a precise calibration of the geothermometer, which doesn't occur in Etnean magmas. For the prehistoric kaersutite (compositions from D'Orazio *et al.*, 1998) relevant geophysical data are missing, leaving some more degrees of uncertainty. Even with these limitations, results obtained from the hornblende geothermometer (Otten, 1984) give a crystallization T of ~ 1025 °C for the prehistoric kaersutite.

The pressure needed for the crystallization of Mg-hastingsite is at least 200 MPa, that might be expected in a closed reservoir subject to a total pressure consistent with a depth of ~ 6 km b.s.l. The distribution of hypocentres for the earthquake swarms, that shortly preceded the eruption onset, indicates a maximum depth of ~ 8 km below the lowest end of the N-S eruptive fracture on the southern flank of the volcano (opened at 2100 m a.s.l.; Bonaccorso *et al.*, 2002; 2004; Patanè *et al.*, 2002; Billi *et al.*, 2003; Lanzafame *et al.*, 2003; Monaco *et al.*, 2005). As a consequence, the relation inferred between the deepest hypocenters and the site of the magma reservoir suggests that the pressure acting on the feeding system during Mg-hastingsite crystallization must have been higher than ~ 200 MPa. Specifically, the maximum depth of hypocentres below the eruptive fracture (8 km) suggests 250−270 MPa as possible values of the confining pressure. Further evidence, which supports the P values inferred from geophysical data, derives from data on H_2O and CO_2 contents of primary melt inclusions in olivine crystals from the lower vent of the 2001 eruption (2100 m a.s.l.; Metrich *et al.*, 2004). These data fit to a melt entrapment under pressures between 200 and 300 MPa, while the olivine crystals were growing, and result in good agreement with the values given above.

The range of pressure values so obtained by these independent approaches is likely depending on the variability of chemical/physical conditions in the magma batch, in particular: 1) a possible vertically extended magma chamber at depths higher than 6 km (b.s.l.) and/or 2) a P_{fluid} increase especially at the top of the magma chamber induced by an upward diffusion of volatiles. This last hypothesis may account for the presence of abundant large Mg-hastingsite megacrysts that occur especially in the early erupted lava

flows, implying that a high growth rate of amphibole was possible at the top of the chamber, probably due to a localized increased P_{fluid} that has led to the development of a "pneumatolytic" environment (*cf.* Pompilio & Rutherford, 2002; Clocchiatti *et al.*, 2004). However, considering that the emission of amphibole-bearing products continued for the total length of the eruption, the hypothesis is highly consistent with the recent results provided by Ferlito *et al.* (2007), who highlighted how the petrological features of the magmas involved in the 2001 event, and coming from the reservoir of the amphibole-bearing trachybasalt, may be constrained only taking into account the role played by migrating volatiles into the feeding system, which have probably led to an overpressurization of the system.

5.4 Crystallization conditions of prehistoric *vs.* recent Etnean amphiboles

Differences in the compositions of Etnean amphiboles are largely related to higher contents of Ti, Na, REE and other trace elements in prehistoric kaersutite and higher contents of Al^{VI}, Ca, K and transition elements in the recent Mg-hastingsite (Fig. 2 and 3). As discussed above, these features may be then accounted for by differences in the chemical and physical parameters, such as melt composition, P, T and fO_2, which control the crystallization.

With regard to magma compositions, kaersutite phenocrysts are commonly found in rather evolved products of the Etnean succession (benmoreites to trachytes), whereas Mg-hastingsite is characteristic of the trachybasalts of the 2001 event. It is noteworthy that this is the first occurrence of an amphibole-bearing magma since the petrological benchmark defined by the 1971 eruption. Many authors focused their attention on the important geochemical changes of the products emitted after the 1971 eruption, and presented various interpretations for explaining the progressive enrichment in K, Rb, Cs joined to a gradually increased $^{87}Sr/^{86}Sr$ value too (Joron & Treuil, 1984; Clocchiatti *et al.,* 1988; Armienti *et al.,* 1989; 2002; Barbieri *et al.,* 1993; Condomines *et al.,* 1995; Tonarini *et al.,* 1995; 2001; Corsaro & Cristofolini 1996; Tanguy *et al.,* 1997; Schiano *et al.,* 2001). More interestingly, other authors have recently pointed out the uncommon features of the eruptive activity of 2001, which could be regarded as a new turning point under several petrological aspects (Clocchiatti *et al.,* 2004; Metrich *et al.,* 2004; Viccaro *et al.,* 2006). After the 2001 eruption, the Etnean magmas have displayed a clear drift of the geochemical features towards more basic, alkali- and volatile-rich members (Clocchiatti *et al.,* 2004; Metrich *et al.,* 2004; Viccaro, 2006; Viccaro *et al.,* 2006; Ferlito *et al.,* submitted). It appears then likely that the observed Mg-hastingsite composition could be significantly depending on these K-enriched and basic magmas.

In contrast to the findings that, at constant magma compositions, Ti and Al^{IV} contents strongly increase with temperature (Heltz, 1973), the relatively higher content of Ti in kaersutite and of Al^{IV} in Mg-hastingsite, as well as the similar growth temperatures estimated for Mg-hastingsite ($T \sim 980$ °C) and kaersutite ($T \sim 1025$ °C), suggest that T did not play a significant role in controlling their compositions. As high Al^{VI} (Deer *et al.*, 1997) and low Ti values (King *et al.*, 2000; Adam & Green, 1994; 2003; Ernst & Liu, 1998) in amphiboles are generally favoured by increased pressures, it seems reasonable that the lower Ti and higher Al^{VI} contents in Mg-hastingsite with respect to kaersutite, as well as $^{Amph/melt}D$ lower in Mg-hastingsite than in kaersutite, could be an effect of different pressures within the magma reservoirs, superimposed to the one due to rather different geochemical characteristics of the melts. Melt compositions and crystallization P can then be viewed as the crucial factors on which the structural and compositional differences among the Etnean amphiboles depend.

6. Concluding remarks

The occurrence of amphibole maintaining its equilibrium with the melt attained at high-P is exceptionally rare in volcanic environments due to the fast re-equilibration under low pressure conditions. The presence of amphibole in trachybasaltic volcanics of the 2001 eruption at Mt. Etna has drawn the attention of many authors (Clocchiatti & Tanguy, 2001; Clocchiatti *et al.*, 2004; Viccaro *et al.*, 2006; Corsaro *et al.,* 2007). The most singular aspect certainly is that, in tephra related to the most violent explosive phases of the event, it preserved the original equilibrium features with the surrounding melt, well represented by the coexisting glass, basaltic-trachyandesite in composition. This has allowed accurate $^{Amph/melt}D$ to be calculated for several trace elements. Even more interestingly, trace element partitioning provides information on the effects that amphibole crystallization exerts on the composition of the residual melts in alkali basaltic systems, suggesting that trace element ratios of great importance in petrology (*e.g.* Th/Ta, U/Ta, Th/Nb, La/Nb) are strongly affected if amphibole fractionation occurs.

Attention was also focused on the fact that amphiboles are fairly rare in the Etnean record and that they are commonly found as kaersutite to titanian pargasite phenocrysts. Efforts have been then made to define which chemical and physical parameter/s should have changed to allow titanian Mg-hastingsite to crystallize in the 2001 eruption reservoir. Mineral-chemical and trace element partitioning data on Mg-hastingsite have been then compared with those reported for the kaersutite of prehistoric eruptions, which provided some constraints for their crystallization. The overall data indicate that compositional differences between Mg-hastingsite and kaersutite are possibly related to the more basic characters of the Etnean magmas erupted in historic time and in particular to the peculiar geochemical features that characterize them after the benchmarks of the 1971 and 2001 events. Combined with this, the behaviour of Ti, Al^{IV}, Al^{VI} and $^{Amph/melt}D$ for trace elements in Mg-hastingsite and kaersutite are consistent with higher pressures of crystallization for the former with respect to the latter. In such a framework, volatile-influx, occurring by diffusion between magma batches within the Etnean feeding system, has been recently indicated as an

efficient process for concentrating anomalous amounts of volatiles and giving rise to high P_{fluid} conditions within closed reservoirs (Ferlito *et al.,* 2007). This mechanism, probably joined to the originally high volatile contents that characterize the recently erupted magmas (Clocchiatti *et al.,* 2004; Metrich *et al.,* 2004; Viccaro, 2006; Viccaro *et al.,* 2006), should have led to attain chemical and physical conditions which locally allowed amphibole to crystallize even from poorly evolved magmas.

Acknowledgements: We would like to express our gratitude to Raul Carampin and Anna Maria Fioretti (CNR-IGG, Unit of Padova) for their support in EMP analyses and to Riccardo Vannucci, Massimo Tiepolo and Alberto Zanetti (Dipartimento di Scienze della Terra, Pavia; CNR-IGG, Unit of Pavia) for having made available labs facilities and for their invaluable technical assistance in LAM-ICP/MS data acquisition. We thank Angelo Peccerillo, Sandro Conticelli, Hilary Downes and an anonymous reviewer for their productive suggestions and insightful reviews that significantly contributed to improve the quality of this work. Authors also acknowledge financial support from INGV-DPC (National Institute for Geophysics and Volcanology-Department of Civil Defence) and MIUR-PRIN Project 2005.

References

Adam, J. & Green, T.H. (1994): The effects of pressure and temperature on the partitioning of Ti, Sr and REE between amphibole, clinopyroxene and basanitic melts. *Chem. Geol.*, **117**, 219-223.

—,— (2003): The influence of pressure, mineral composition and water on trace element partitioning between clinopyroxene, amphibole and basanitic melts. *Eur. J. Min.*, **15**, 831-841.

Anders, E. & Ebihara, M. (1982): Solar system abundances of the elements. *Geoch. Cosmoch. Acta*, **46**, 2363-2380.

Aoki, K. (1963): The kaersutites and oxykaersutites from alkalic rocks of Japan and surrounding areas. *J. Petrol.*, **4**, 198-210.

Armienti, P., Innocenti, F., Petrini, R., Pompilio, M., Villari, L. (1989): Petrology and Sr-Nd isotope geochemistry of recent lavas from Mt. Etna: bearing on the volcano feeding system. *J. Volcanol. Geotherm. Res.*, **39**, 315-327.

Armienti, P., Tonarini, S., D'Orazio, M., Innocenti, F. (2002): Genesis and evolution of Mt. Etna alkaline lavas: petrological and Sr-Nd-B isotope constraints. *Per. Mineral.*, **73**, 29-52.

Baker, I. (1969): Petrology of the volcanic rocks of Saint Helena Island, South Atlantic. *Bull. Geol. Soc. Am.*, **80**, 1283-1310.

Barbieri, M., Cristofolini, R., Delitala, M.C., Fornaseri, M., Romano, R., Taddeucci, A., Tolomeo, L. (1993): Geochemical and Sr-isotope data on historic lavas of Mount Etna. *J. Volcanol. Geotherm. Res.*, **56**, 57-69.

Barclay, J. & Carmichael, I.S.E. (2004): A hornblende basalt from Western Mexico: water-saturated phase relations constrain a pressure-temperature window of eruptibility. *J. Petrol.*, **45**, 485-506.

Billi, A., Acocella, V., Funiciello, R., Giordano, G., Lanzafame, G., Neri, M. (2003): Mechanism for ground-surface fracturing and incipient slope failure associated with the 2001 eruption of Mt. Etna, Italy: analysis of ephemeral field data. *J. Volcanol. Geotherm. Res.*, **22**, 281-294.

Bonaccorso, A., Aloisi, M., Mattia, M. (2002): Dike emplacement forerunning the Etna July 2001 eruption modelled through continuous tilt and GPS data. *Geophys. Res. Lett.*, **29** (2), 1-4.

Bonaccorso, A., D'Amico, S., Mattia, M., Patanè, D. (2004): Intrusive mechanism at Mt. Etna forerunning the July – August 2001 eruption. *Pure Appl. Geophys.*, **161** (7), 1469-1487.

Bottazzi, P., Tiepolo, M., Vannucci, R., Zanetti, A., Brumm, R., Foley, S.F., Oberti, R. (1999): Distinct sites preferences for heavy and light REE in amphibole and the prediction of $^{Amph/L}D_{REE}$. *Contr. Mineral. Petrol.*, **137**, 36-45.

Browne, B.L., Eichelberger, J.C., Patino, L.C., Vogel, T.A., Uto, K., Hoshizumi, H. (2006): Magma mingling as indicated by texture and Sr/Ba ratios of plagioclase phenocrysts from Unzen volcano, SW Japan. *J. Volcanol. Geotherm. Res.*, **154**, 103-116.

Clocchiatti, R. & Tanguy, J.C. (2001): Amphibole megacrysts from the 2001 S-flank eruption, Etna, Italy. *Bull. Global Volc. Network Smithson. Inst.*, **26** (10), 3-4.

Clocchiatti, R., Joron, J.L., Treuil, M. (1988): The role of selective alkali contamination in the evolution of recent historic lavas of Mt. Etna. *J. Volcanol. Geotherm. Res.*, **34**, 241-249.

Clocchiatti, R., Condomines, M., Guènot, N., Tanguy, J.C. (2004): Magma changes at Mount Etna: the 2001 and 2002−2003 eruptions. *Earth Plan. Sci. Lett.*, **226**, 397-414.

Condomines, M., Tanguy, J.C., Michaud, V. (1995): Magma dynamics at Mt Etna: constraints from U-Th-Ra-Pb radioactive disequilibria and Sr isotope in historical lavas. *Earth Plan. Sci. Lett.*, **132**, 25-41.

Corsaro, R.A. & Cristofolini, R. (1996): Origin and differentiation of recent basaltic magmas from Mount Etna. *Mineral. Petrol.*, **57**, 1-21.

Corsaro, R.A., Miraglia, L., Pompilio, M. (2007): Petrologic evidence of a complex plumbing system feeding the July–August 2001 eruption of Mt. Etna, Sicily, Italy. *Bull. Volcanol.*, **69**, 401-421.

Couch, S., Harford, C.L., Sparks, R.S.J., Carroll, M.R. (2003): Experimental constraints on the conditions of formation of highly calcic plagioclase microlites at the Soufriere Hills Volcano, Montserrat. *J. Petrol.*, **44**, 1455-1475.

Cristofolini, R. & Lo Giudice, A. (1969): Ricerche su due kaersutiti etnee. *Atti Acc. Gioenia Sci. Nat.*, **20**, 181-193.

Cristofolini, R., Scribano, V., Tranchina, A. (1981): Interpretazione petrogenetica di variazioni composizionali in fenocristalli femici di lave etnee. *Rend. Soc. Ital. Mineral. Petrol.*, **31**, 309-336.

Deer, W.A., Howie, R.A., Zussman, J. (1997): Rock-forming minerals – Double chain silicates (Second Ed.). Published by Geol. Soc. London, 135-613.

Devine, J.D., Rutherford, M.J., Norton, G.E. (2003): Magma storage region processes inferred from geochemistry of Fe-Ti oxides in andesitic magma, Soufrière Hills volcano, Montserrat, W.I. *J. Petrol.*, **44**, 1375-1400.

D'Orazio, M., Armienti, P., Cerretini, S. (1998): Phenocryst/matrix trace-element partition coefficients for hawaiite-trachyte lavas from the Ellittico volcanic sequence (Mt. Etna, Sicily, Italy). *Min. Petrol.*, **64**, 65-88.

Downes, H., Beard, A., Hinton, R. (2004): Natural experimental charges: an ion-microprobe study of trace element distribution coefficients in glass-rich hornblendite and clinopyroxenite xenoliths. *Lithos*, **75**, 1-17.

Ernst, W.G. & Liu, J. (1998): Experimental phase-equilibrium study of Al- and Ti-content of calcic amphibole in MORB – a semi-quantitative thermobarometer. *Am. Miner.*, **83**, 952-969.

Ferlito, C., Viccaro, M., Cristofolini, R. (2007): Magma differentiation induced by volatile migration in the shallow plumbing system of active volcanoes: evidence from the 2001 eruption at Mt. Etna (Italy). *Geophys. Res. Abs.*, **9**, 04183, SRef-ID: 1607-7962/gra/EGU2007-A-04183.

Fisher, R.V. & Schmincke, H.U. (1984): Pyroclastic rocks. Springer, Berlin-Heidelberg-New York-Tokyo, pp. 1-472.

—,— (1994): Volcanic sediment transport and deposition. In: Sedimentary processes. Pye K (Ed.), Blackwell, Oxford, pp. 349-386.

Gast, P.W. (1968): Trace element fractionation and the origin of tholeiitic and alkaline magma types. *Geoch. Cosmoch. Acta*, **32**, 1057-1086.

Green, T.H. & Pearson, N.J. (1985): Experimental determination of REE partition coefficients between amphibole and basaltic to andesitic liquids at high pressure. *Geoch. Cosmoch. Acta*, **49**, 1465-1468.

Griffin, W.L. & Murthy, V.R. (1969): Distribution of K, Rb, Sr, and Ba in some minerals relevant to basalt genesis. *Geoch. Cosmoch. Acta*, **33**, 1389-1414.

Heltz, R.T. (1973): Phase relations of basalts in their melting range at P_{H_2O} = 5 Kb as a function of oxygen fugacity (Part 1). *J. Petrol.*, **14**, 249-302.

Higuchi, H. & Nagasawa, H. (1969): Partition of trace elements between rock-forming minerals and the host volcanic rocks. *Earth Plan. Sci. Lett.*, **7**, 281-287.

Irving, A.J. & Frey, F.A. (1984): Trace element abundances in megacrysts and their host basalts: constraints on partition coefficients and megacryst genesis. *Geoch. Cosmoch. Acta*, **48**, 1201-1221.

Jeffries, T.E., Jackson, S.E., Longerich, H.P. (1998): Application of a frequency quintupled Nd: YAG source (l = 213 nm) for laser ablation inductively coupled plasma mass spectrometric analysis of minerals. *J. Anal. Atomic Spectr.*, **13**, 935-940.

Joron, J.L. & Treuil, M. (1984): Etude geochimique et petrogenese des laves de l'Etna, Sicilie (Italie). *Bull. Volcanol.*, **47**, 1125-1144.

Kesson, S. & Price, R.C. (1972): The major and trace element chemistry of kaersutite and its bearing on the petrogenesis of alkaline rocks. *Contr. Mineral. Petrol.*, **35**, 119-124.

King, P.L., Hervig, R.L., Holloway, J.R., Delaney, J.S., Dyar, M.D. (2000): Partitioning of Fe^{3+}/Fe_{total} between amphibole and basanitic melt as a function of oxygen fugacity. *Earth. Plan. Sc. Lett.*, **178**, 97-112.

Klerkx, J. (1964): Sur la presence de Syntagmatite à l'Etna. *Ann. Soc. Geol. Belg.*, **87**, 147-157.

— (1968): Etude geologique et petrologique de la Valle del Bove (Etna). PhD Thesis, Universitè de Liege.

Lanzafame, G., Neri, M., Acocella, V., Billi, A., Funiciello, R., Giordano, G. (2003): Structural features of the July-August 2001 Mount Etna eruption evidence for a complex magma supply system. *J. Geol. Soc. London*, **160**, 531-544.

LaTourrette, T., Hervig, R.L., Holloway, J.R. (1995): Trace element partitioning between amphibole, phlogopite and basanite melt. *Earth Plan. Sci. Lett.*, **135**, 13-30.

Leake, B.E. (1978): Nomenclature of amphiboles. *Canad. Mineral.*, **16**, 501-520.

Leake, B.E., Woolley, A.R., Arps, C.E.S., Birch, W.D., Gilbert, M.C., Grice, J.D., Hawthorne, F.C., Kato, A., Kisch, H.J., Krivovichev, V.G., Lunthout, K., Laird, J., Mandarino, J., Maresch, W.V., Nickel, E.H., Rock, N.M.S., Schumacher, J.C., Smith, D.C., Stephenson, N.C.N., Ungaretti, L., Whittaker, E.J.W., Youzhi G. (1997): Nomenclature of Amphiboles: report of the subcommittee on amphiboles of the international mineralogical association, commission on new minerals and mineral names. *Canad. Mineral.*, **35**, 219-246.

Le Maitre, R.W. (1962): Petrology of volcanic rocks, Gough Islands, South Atlantic. *Bull. Geol. Soc. Am.*, **73**, 1309-1340.

— (1969): Kaersutite-bearing xenoliths from Tristan da Cunha. *Mineral. Mag.*, **37**, 185-197.

— (2002): A classification of igneous rocks and glossary of terms. Cambridge University Press, 236 pp.

Lemarchand, F., Villemant, B., Calas, G. (1987): Trace element distribution coefficients in alkaline series. *Geoch. Cosmoch. Acta*, **51**, 1071-1081.

Lopez, M., Pompilio, M., Rotolo, S.G. (2006): Petrology of some amphibole-bearing volcanics of the pre-Ellittico period (102-80 ka), Mt. Etna. *Per. Mineral.*, **75**, 151-166.

Metrich, N., Allard, P., Spilliaert, N., Andronico, D., Burton, M. (2004): 2001 flank eruption of the alkali- and volatile-rich primitive basalt responsible for Mount Etna's evolution in the last three decades. *Earth Plan. Sc. Lett.*, **228**, 1-17.

Monaco, C., Catalano, S., Cocina, O., De Guidi, G., Ferlito, C., Gresta, S., Musumeci, C., Tortorici, L. (2005): Tectonic control on the eruptive dynamics at Mt. Etna Volcano (Sicily) during the 2001 and 2002–2003 eruptions. *J. Volcanol. Geotherm. Res.*, **144**, 211-233.

Mysen, B.O. & Virgo, D. (1980): Trace element partitioning and melt structure: an experimental study at 1 atm. *Geoch. Cosmoch. Acta*, **44**, 1917-1930.

Nakagawa, M., Wada, K., Wood, P. (2002): Mixed magmas, mush chambers and eruption triggers: evidence from zoned clinopyroxene phenocrysts in andesitic scoria from the 1995 eruptions of Ruapehu volcano, New Zealand. *J. Petrol.*, **43**, 2279-2303.

Nicholls, I.A. & Harris, K.L. (1980): Experimental rare earth element partition coefficients for garnet, clinopyroxene and amphibole coexisting with andesitic and basaltic liquids. *Geoch. Cosmoch. Acta*, **44**, 287-308.

Otten, M.T. (1984): The origin of brown hornblende in the Artfjallet gabbro and dolerites. *Contr. Min. Petrol.*, **86**, 189-199.

Patanè, D., Chiarabba, C., Cocina, O., De Gori, P., Moretti, M., Boschi, E. (2002): Tomographic images and 3D earthquake locations of the seismic swarm preceding the 2001 Mt. Etna eruption: evidence for a dyke intrusion. *Geophys. Res. Lett.*, **29** (135), 1-4.

Pearce, J.A. & Norry, M.J. (1979): Petrogenetic implications of Ti, Zr, Y and Nb variations in volcanic rocks. *Contr. Min. Petrol.*, **69**, 33-47.

Pompilio, M. & Rutherford, M.J. (2002): Pre-eruption conditions and magma dynamics of recent amphibole-bearing Etna basalt. *Eos Trans. AGU, Fall Meeting Supplement*, **83**, 47-F1419.

Reubi, O., Nicholls, I.A., Kamenetsky, V.S. (2002): Early mixing and mingling in the evolution of basaltic magmas: evidence from phenocryst assemblages, Slamet Volcano, Java, Indonesia. *J. Volcanol. Geotherm. Res.*, **119**, 255-274.

Rutherford, M.J. & Devine, J.D. (2003): Magmatic conditions and magma ascent as indicated by hornblende phase equilibria and reactions in the 1995-2002 Soufrière Hills magma. *J. Petrol.*, **44**, 1433-1454.

Sato, H., Nakada, S., Fujii, T., Nakamura, M., Suzuki-Kamata, K. (1999): Groundmass pargasite in the 1991−1995 dacite of Unzen volcano: phase stability experiments and volcanological implications. *J. Volcanol. Geotherm. Res.*, **89**, 197-212.

Schiano, P., Clocchiatti, R., Ottolini, L., Busà, T. (2001): Transition of Mount Etna lavas from a mantle-plume to an island-arc magmatic source. *Nature*, **412**, 900-904.

Sisson, T.W. (1994): Hornblende-melt trace-element partitioning measured by ion microprobe. *Chem. Geol.*, **117**, 331-344.

Sun, S.S. (1982): Chemical composition and origin of the Earth's primitive mantle. *Geoch. Cosmoch. Acta*, **46**, 179-192.

Sun, S.S. & McDonough, W.F. (1989): Chemical and isotopic systematic of oceanic basalts: implications for mantle composition and processes. *in*: "Magmatism in ocean basins", Saunders, A.D. & Norry, M.J. (eds.). Geol. Soc. London. Spec. Pub., **42**, 313-345.

Taddeucci, J., Pompilio, M., Scarlato, P. (2004): Conduit processes during the July-August 2001 explosive activity of Mount Etna (Italy): inferences from glass chemistry and crystal size distribution of ash particles. *J. Volcanol. Geotherm. Res.*, **137**, 33-54.

Tanguy, J.C. (1980): L'Etna, etude petrologique et paleomagnetique: implications volcanologiques. PhD Thesis, Université Pierre et Marie Curie, Paris 6 (France).

Tanguy, J.C., Condomines, M., Kieffer, G. (1997): Evolution of Mount Etna magma: Constraints on the present feeding system and eruptive mechanism. *J. Volcanol. Geotherm. Res.*, **75**, 221-250.

Tiepolo, M., Vannucci, R., Oberti, R., Foley, S.F., Bottazzi, P., Zanetti, A. (2000): Nb and Ta incorporation and fractionation in titanian pargasite and kaersutite: crystal-chemical constraints and implications for natural systems. *Earth Plan. Sci. Lett.*, **176**, 185-201.

Tiepolo, M., Bottazzi, P., Foley, S.F., Oberti, R., Vannucci, R., Zanetti, A. (2001): Fractionation of Nb and Ta from Zr and Hf at mantle depths: the role of titanian pargasite and kaersutite. *J. Petrol.*, **42**, 221-232.

Tonarini, S., Armienti, P., D'Orazio, M., Innocenti, F., Pompilio, M., Petrini, R. (1995): Geochemical and isotopic monitoring of Mt. Etna 1989 – 1993 eruptive activity: bearing on the shallow feeling system. *J. Volcanol. Geotherm. Res.*, **64**, 95-115.

Tonarini, S., Armienti, P., D'Orazio, M., Innocenti, F. (2001): Subduction-like fluids in the genesis of Mt. Etna magmas: evidence from boron isotopes and fluid mobile elements. *Earth Plan. Sci. Lett.*, **192**, 471-483.

Viccaro, M. (2006): Genesis, differentiation and eruptive dynamics of Mt. Etna magmas. PhD Thesis, University of Catania (Italy).

Viccaro, M., Ferlito, C., Cortesogno L., Cristofolini, R., Gaggero, L. (2006): Magma mixing during the 2001 event at Mt. Etna (Italy): effects on the eruptive dynamics. *J. Volcanol. Geoth. Res.*, **149**, 139-159.

Received 10 May 2006
Modified version received 23 April 2007
Accepted 24 May 2007